TII-18-2286 IEEE Transactions on Industrial Informatics, Volume 15, Issue 1, January 2019, pp. 445-453 1
DOI:10.1109/TII.2018.2878758

Estimation of Damage Thickness in Fibre-reinforced Composites using Pulsed Thermography

Adisorn Sirikham, Yifan Zhao*, Hamed Yazdani Nezhad, Weixiang Du, and Rajkumar Roy

***Abstract*—Non-destructive-testing (NDT), including active thermography, has become an inevitable part of composite process and product verification, post-manufacturing. However, there is no reliable NDT technique available to ensure the interlaminar bond integrity during composite laminates integration, bonding or repair where the presence of thin airgaps in the interface of dissimilar polymer composite materials would be detrimental to structural integrity. This paper introduces a novel approach attempting to quantify the damage thickness of composites (the thickness of air gaps inside composites) through a single-side inspection of pulsed thermography. The potential of this method is demonstrated by testing on three specimens with different types of defect, where the Pearson Correlation Coefficients of the thickness estimation for block defects and flat-bottom holes are 0.75 and 0.85, respectively. This approach will considerably enhance the degradation assessment performance of active thermography by extending damage measurement from currently two dimensions to three dimensions, and become an enabling technology on quality assurance of structural integrity.**

***Index Terms*—Active thermography, composite damage detection, bonded repair, nonlinear system identification, correlation analysis**

I. Introduction

THE effect of bond defects on the strength and toughness of adhesively bonded composite joints (e.g. due to contamination, improper surface treatment or shrinkage during polymer cure) can become considerable, and under severe circumstances may lead to catastrophic failure of the joints [1]. Although nowadays non-destructive testing (NDT) is commonly used to inspect defects/damage of composite process and product verification during post-manufacturing and in operation, there is no reliable NDT technique available to ensure the bond integrity i.e. via detecting nearly zero-thickness defects that may represent thin airgaps in the interface of dissimilar polymer composite materials [2]. A number of researches have recently focused on the identification and evaluation of unknown interaction between inspection of bond defects in composite-to-composite bonded joints and their effect on the ultimate strength of the joints [1], [3]. They have observed that the existing NDT techniques (e.g. ultrasound) are not capable of detecting bond defects and narrow airgaps caused by improper composite processing while such defects may result in more than 40% reduction in the joints strength. This becomes one of the most significant challenges in structural bonding applications, for instance in aerospace, where strict certifications (e.g. FAA Advisory Circular 20-107B) do not allow bonded composite structures unless a certain level of reliability is achieved via NDT, in order to ensure the bond effectiveness after composite joining process. As a result of not having such reliable techniques, the certification suggests that the primary aircraft structures considered for bonded integration or repair must be capable of enduring design limit loads even if the bonded joint fails completely. Airgap defects may also be introduced during low-velocity impact damage where instantaneously occurring interlaminar delamination becomes the dominant mechanism with more than 60% dissipation of impact energy [4], [5], and as such while the damage is barely visible via NDT techniques, it could result in catastrophic failure of the composite structure if not detected and repaired.

Majority of NDT research focus on measuring the location and sizes of defects or damages, but limited studies on characterisation of their thickness. Microwave thermography has been used to study the effect of corrosion layer thickness on reinforcing steel bars [6], [7], but has not been applied on composites. Wang *et al.* proposed a microwave equiphase frequency truncation method to detect and evaluate the thickness of kissing defects in GFRP laminate [8]. Pulsed Eddy Current technique has been used in thickness evaluation of aluminium plate [9], and the ultrasonic testing has been widely used for gauging of the local thickness of a solid element [10], but very limited related research for the sub-surface defect or damages. X-ray computed tomography is able to provide highly accurate 3D inspections of manufacturing defects of fibre architectures [11], however the inspection time and equipment is relatively costly.

As a highly efficient and powerful NDT technique, Pulsed Thermography is contact-free and offers a rapid inspection while covering a large area within a short time frame and thus readily adaptable to in-situ monitoring applications [12]. Other thermography-based NDTs, such as microwave thermography, eddy current thermography, lock-in thermography, and

Manuscript submitted November 29, 2017; revised July 12, 2018 and August 16, 2018; accepted October 15, 2018.

All authors are with the School of Aerospace, Transport and Manufacturing, Cranfield University, College Road, Cranfield, Bedfordshire, MK43 0AL, UK.

*Corresponding author: Yifan Zhao (e-mail: yifan.zhao@cranfield.ac.uk).

ultrasonic thermography, takes several measurements using signals of different frequencies to gain information about different depths, however it requires a longer inspection time. Pulsed thermography is more straightforward and faster because the flash time is a well-defined instant for time reference. Quantitative characterisation of defects by extracting shape, size and depth have been well-studied and proven to be effective by Pulsed Thermography [13], [14]. Most of the existing methods, such as Peak Slope Time [15], Logarithm Second Derivative [16], Absolute Peak Slope Time [17], Nonlinear System Identification [18], Least Square Fitting [19], and New Least Square Fitting [20], are able to estimate the defect depth (the distance from the inspected surface to the top surface of a defect) before the three-dimensional heat conduction takes place. However, currently characterisation of defects is limited to 2-dimensional measurement, which represents a collation of all damage through-the-thickness. None of these method is able to measure the defect thickness in order that the measurement can be extended to 3-dimension. A straightforward approach to tackle this challenge is conducting two inspections, one of which is applied on the front side and another on the rear side. The defect thickness can then be quantified by considering the measured defect depths from both inspections and the sample thickness. However, the application of this approach is limited because a) one side of the inspected component could be inaccessible e.g. an aircraft wing or fuselage, b) the accuracy of measurement could be compromised if the defect thickness is very thin due to extreme closed values of defect depth from two inspections, and c) it introduces extra cost of inspection time. This paper aims to introduce a novel approach to quantify the damage thickness of composites based on a single inspection of pulsed thermography.

II. Methods

A. Pulsed thermography

In pulsed thermographic inspection working under the reflection mode, the typical experimental setup of which is illustrated by Fig. 1(a), a short and high energy light pulse from the flash lamps is projected onto the sample surface. Heat conduction then takes place from the heated surface to the interior of the sample, leading to a continuous decrease of the surface temperature. An infrared (IR) radiometer controlled by a computer captures the time-dependent response of the sample surface temperature. In areas of the sample surface above a defect/damage (see the point 2 in Fig. 1) the transient flow of heat from the surface into the sample bulk is wholly or partially obstructed, thus causing a temperature deviation from the sound areas (see the point 1 in Fig. 1). Fig. 1(b) plots two typical observed temperature decay curves of the point 1 (blue) and 2 (red) in the logarithmic domain. Damage detection methods aims to classify the pixels based on the cooling behaviour. The time when the temperature deviation occurs, represented by t* in Fig. 1(b), is usually used to estimate the defect depth d. On a sufficiently large time scale, the t* can be viewed as a transition from 1-dimensional steady state diffusion before incident heat encounters a subsurface interface to a second asymptotic steady state [15]. We can also observe a later event t** (see in Fig. 1(b)), indicating the asymptotic return to 1-dimensional diffusion. The detection of t* and t** can be achieved through detecting the peak of the second derivative of TSR [21]. The cooling behaviour between t* to t** is associated with the size r, the depth d, the thickness h of damage and the material, as labelled in Fig. 1(a). Estimation and understanding of the corresponding between them is the key to characterise the volume of damage and will be studied in this paper.

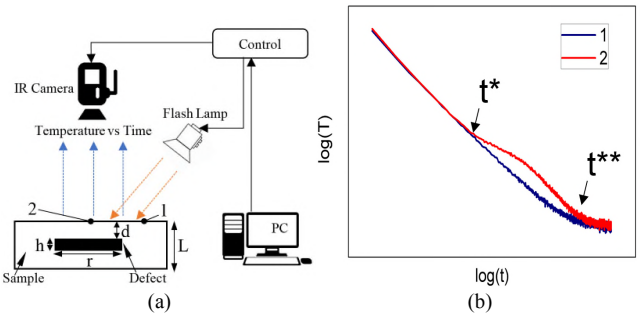

(a) (b)

Fig. 1. (a) Experimental configuration of the pulsed thermographic inspection under the reflection mode. (b) Typical observed time-temperature decay curves in the logarithmic domain for the point 1 and 2, respectively.

B. Estimation of thermal reflection coefficient

The surface temperature dynamics due to the back-wall at depth L for a homogeneous plate is given by [22]:

$$T(t) = \frac{Q}{\sqrt{\pi\rho ckt}}\left[1 + 2\sum_{n=1}^{\infty} R^n \exp\left(-\frac{n^2L^2}{\alpha t}\right)\right], \quad (1)$$

where $T(t)$ is the temperature variation of the surface at time t, Q is the pulse energy, ρ is the material density, c is the heat capacity, k is the thermal conductivity of the material, R is the thermal reflection coefficient of the interface with air, and α is the thermal diffusivity. For most of research the value of R in (1) is assumed to be 1, which is true when the thickness or the size of damage (e.g. air gap) is infinite, where there is no three-dimensional heat conduction takes place. However, for most of the real applications (e.g. detecting impact damage of composite), the thickness and size of damage could be very small and the heat leakage can be severe. The value of R therefore can be significantly smaller than 1 [23] if the whole transient lifetime is considered. By monitoring the cooling temperature during the period from the flash time to t**, this paper proposes to characterise the damage thickness through establishing an empirical model between R and measurable geometrical parameters.

This paper proposes to use the New Least-Squares Fitting method proposed by Sirikham *et al.* [23] to estimate the R value directly from the observed data. The NLSF method introduces an analytical model, written as

$$\tilde{T}(t, A, W, R, t_s, s) = \frac{A}{\sqrt{t+t_s}}\left[1 + 2\sum_{n=1}^{M} R^n \exp\left(-\frac{n^2W}{t+t_s}\right)\right] - s(t + t_s), \quad (2)$$

where $A = \frac{Q}{\sqrt{\pi\rho ck}}$, $W = \frac{L^2}{\alpha}$, t_s is the starting time of sampling, and M is a large number to replace the infinite symbol (∞) in

Eq. (1) for the implementation in Matlab. In this paper M was chosen as 1000. Values of M larger than 1000 have been tested and there is no influence on the results. There are five unknown parameters including t_s, R, W, A and s. A nonlinear least-squares solver in Matlab (*lsqnonlin*) is then used to solve this five-parameters optimisation problem. Through initially setting the lower and upper bounds for each parameter, this method estimates the optimal parameters to achieve

$$\min_{A,W,R,t_s,s} \left\| \tilde{T}(t, A, W, R, t_s, s) - T(t) \right\|. \quad (3)$$

The initial value of the parameter t_s is selected as zero and the lower and upper bounds are selected as -1 and 1 respectively because it is usually very close to zero. The initial value of R is selected as 1 and the lower and upper bounds are selected as 0 and 1 respectively. The selection of A depends on the energy applied on the inspection surface, and the selection of W depends on the material and thickness of samples. The lower and upper bounds of W and A are usually selected as 5 times lower and 5 times higher than the initial values. The lower and upper bounds of s are selected as -50 and 50, and the initial value is chosen as 0. Equation (2) introduces two parameters R and s that consider the three-dimensional heat conduction effect. It can also incorporate the duration effect of flash by introducing the parameter t_s.

C. Correlation analysis and modelling

It has been mentioned above that the R value could be related to geometrical parameters including defect size, depth and thickness. This section aims to introduce an approach to quantify correlations between R and these parameters and identify an empirical model to establish their relationship, by which means the defect thickness can be inferred if R and other two parameters are measurable. From the system engineering point of view, to study this multiple-input single-output correlation, the simplest approach is to fix two inputs and vary the third input, and then evaluate this input's influence on the output (R). The problem is now simplified to study a single-input single-output system. Least square fitting approaches, based on either linear or nonlinear models, can be employed to establish the relationship between R and the third input. This procedure can then be repeated until the relationship between R and each geometrical parameter is studied.

To consider the compound influence of these three parameters on R, their relationship must be considered as a multi-input single-output problem. Considering a system with three inputs u_1, u_2, u_3 and an output y, to describe their relationship, this paper proposes to use the Nonlinear Finite Impulse Response (NFIR) model, written as

$$y = f(u_1, u_2, u_3) + \varepsilon, \quad (4)$$

where f is some unknown linear or non-linear mapping, which links the system output to the system inputs; ε denotes the model residual. A commonly employed model type to specify the function f in (4) is a polynomial function [24], [25]. A second order polynomial function can be written as

$$y = \theta_0 + \theta_1 u_1 + \theta_2 u_2 + \theta_3 u_3 + \theta_4 {u_1}^2 + \theta_5 {u_2}^2 + \theta_6 {u_3}^2 + \theta_7 u_1 u_2 + \theta_8 u_1 u_3 + \theta_9 u_2 u_3. \quad (5)$$

The next step is to estimate the parameters $\theta_m (m = 0,1, \dots, 9)$ based on the observations $\{y, u_1, u_2, u_3\}$. The procedure begins by determining the structure, or the important model terms, using the orthogonal least squares (OLS) estimation procedures. More detailed description of this method can be found in the work of Zhao *et al.* [26].

As a feasibility study, this paper focuses on inspecting commonly studied defects including flat bottom holes and block defects. Considering a block defect as shown in Fig. 1(a), the defect size r, depth d and thickness h are considered as the system inputs, and the value of R is considered as the output. Through establishing a NFIR model, the influence of r, d and h on R will be evaluated initially. An inverse model, written as

$$h = f(R, d, r), \quad (6)$$

can then be inferred to reconstruct h based on r, d and R.

III. Experiments

A. Sample design

Flat plates of carbon fibre reinforced polymer (CFRP) material were used in this study. The plates were made of unidirectional Toray 800 carbon fibres pre-impregnated with Hexcel M21 epoxy resin and manufactured in a traditional autoclaving process. Based on this material, three samples were designed to simulate different type of defect. The dimension of the Sample 1 is 75 mm × 230 mm × 8 mm. As illustrated by Fig. 2, it includes five block defects with a thickness (h) of 0.5 mm, 1.0 mm, 2.0 mm, 3.0 mm, and 4.0 mm respectively. The width (r), length, and depth (d) for all defects are 10 mm, 75 mm, and 2 mm respectively. The distance between two adjacent defects is 30 mm, which aims to reduce the influence from the adjacent defects on the thermal behaviour. A side view of the produced sample is shown in Fig. 2(b). It should be noted that these defects are not fully closed because two sides of the defects are open. It is called as "semi-closed defect". This sample is aimed at studying the relationship between R and h when d is fixed. The Sample 2 also include five semi-closed defects, as illustrated by Fig. 3, which have the same defect thickness h of 1.5 mm but different defect depth of 1.0 mm, 1.5 mm, 2.0 mm, 2.5 mm, and 3.0 mm respectively. Other parameters are same as the Sample 1. This sample is aimed at evaluating the relationship between R and d when h is fixed. The Sample 3, with the dimension of 155 mm × 155 mm × 8 mm, includes 16 flat-bottom holes. As illustrated by Fig. 4(a), the holes were drilled with four groups of diameters (5 mm, 10 mm, 15 mm, and 20 mm) and four groups of thicknesses (7 mm, 6 mm, 5 mm, and 4 mm). It can be inferred that the defect depths are 1 mm, 2 mm, 3 mm, and 4 mm respectively. The distance between the centre of two adjacent holes is 31 mm. This sample is aimed at studying the relationship between R, h, d and r for "open defect". It should be noted that for this sample

the parameters *h* and *d* are dependent and the sum of them is a constant (8 mm).

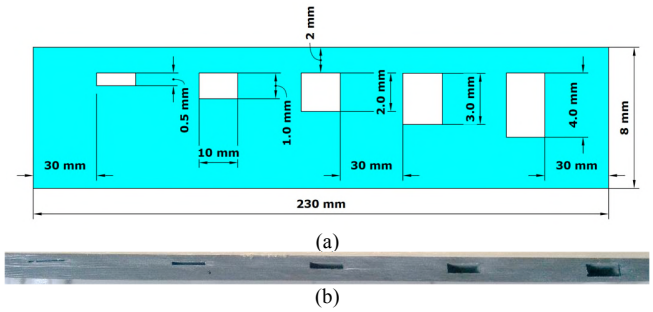

Fig. 2. An illustration of the Sample 1, where the defect size, depth anc thickness are defined. (a) sample design; (b) the side view.

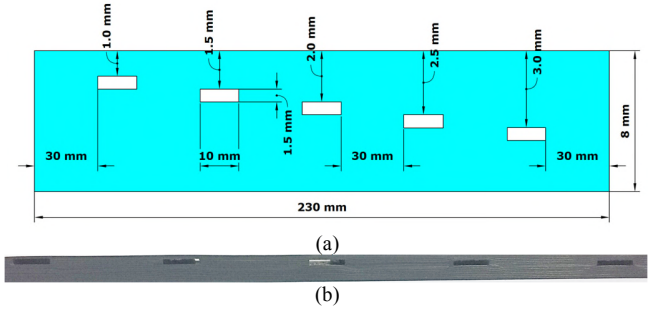

Fig. 3. An illustration of the Sample 2. (a) sample design; (b) the side view.

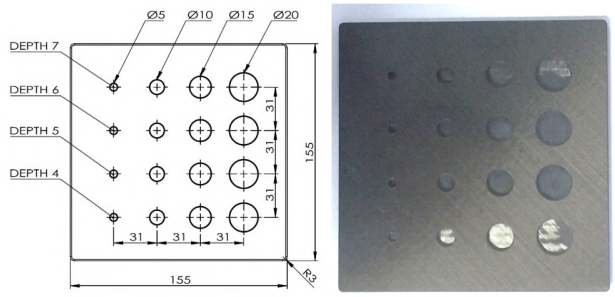

Fig. 4. An illustration of the Sample 3. (a) sample design; (b) the side view.

B. *Experiment setting*

The experiments were conducted using the Thermoscope® II pulsed-active thermography system that comprises of two capacitor banks powered Xenon flash lamps mounted in an internally reflective hood and a desktop PC to capture and store data. The scheme of the experimental set-up is illustrated in Fig. 1(a). A FLIR SC7000 series infrared (IR) radiometer operating between 3-5.1 μm and a spatial resolution of 640×512 pixels was used to perform the inspection. The samples were placed with their surface perpendicular to the IR camera's line of sight at 250 mm from the lens. The apply energy was approximately 2 kJ over an inspection area of 250 mm × 200 mm. The pixel pitch is 0.32 mm. The Sample 1 and the Sample 2 were inspected from the top side of Fig. 2 and Fig. 3. The sample 3 was inspected from the surface opposite to the drilled side. Considering the thickness of the samples and the low thermal diffusivity of CFRP, a sampling rate of 10 Hz was used, and totally 900 frames, equally 90 s data length, were captured. Due to the large width of the Sample 1 and the Sample 2 (230 mm), the defects of both samples suffer non-uniform heating for a single inspection, which could lead to unreliable results [27]. In this study, to reduce this effect, each sample has been inspected for five times, where each defect was placed on the centre of the camera's view once. A region of interest of the centralised defect with the size of 160×120 pixels for five data files was then cropped and merged into one file with a size of 160×600 pixels for easier analysis.

IV. Results

A. *Results of the Sample 1*

Fig. 5 shows a snapshot of the raw thermal image at time 10 s where the colour represents the temperature. It should be noted that the exported data of the used IR camera is in the unit of 'digital intensity', which was used for the analysis below instead of temperature. To reduce the influence of the heat leaked to each opened side on results, ten pixels on the centre of each defect were sampled, as marked in Fig. 5, and then were averaged to reduce spatial noise. The defects are labelled as "(1)", "(2)", "(3)", "(4)", and "(5)" to represent the defect thickness of 0.5 mm, 1.0 mm, 2.0 mm, 3.0 mm, and 4.0 mm respectively, and the sampled sound area is marked as 'S'. Ten pixels (1×10) for each defect and the selected sound area were sampled, and the temperature decays are plotted in the logarithmic domain, as shown in Fig. 6. Considering that the thermal behaviour of sound area around the centre has a very limited variation for the five tests, in this paper the sound area was selected on the first test only. It can be clearly observed that the time of the temperature deviation from the curve of the sound pixel occurs for each defect (t*) is similar since they have the same depth. The thermal cooling behaviours before t* are almost identical, while after t* they start to exhibit difference. Quantification of the influence of the defect thickness on thermal cooling behaviours purely based on the observation of these plots is almost impossible.

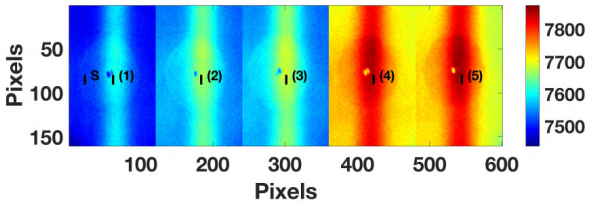

Fig. 5. A snapshot of the captured thermal image of at time 10 s for the Sample 1, where the unit is digital intensity, a representation of temperature. The markers illustrate the 10 sampled pixels of each defect and sound area.

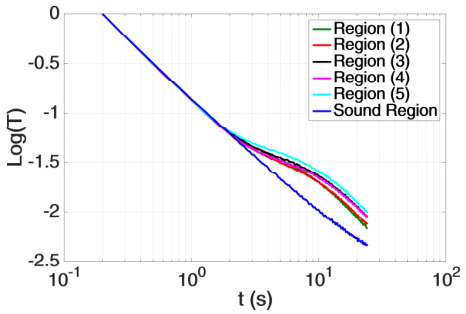

Fig. 6. The average temperature decay, plotted in the logarithmic domain, for the sampled pixels of each defect and a sound region of the Sample 1 The sampled total data length is 24 s.

TABLE I
ESTIMATED PARAMETERS OF THE SAMPLE 1

Defect thickness (mm)	R	d (mm)
0.5	0.431	1.896
1.0	0.498	2.079
2.0	0.565	1.985
3.0	0.588	2.072
4.0	0.591	1.866

The NLSF method was then applied on each time-temperature decay data to estimate the unknown parameters. The thermal diffusivity α was chosen as 0.5×10^{-6} m^2/s, and the measured values of R and d are shown in Table I. It can be calculated that the average measured depth is 1.989±0.098 mm and the average percentage error is about 5% against the reference of 2 mm, which suggests a fine performance of depth estimation. Table I also indicates that the value of R increases following the increase of defect thickness, although the relationship is not linear. This interesting observation is probably caused by that the heat is more difficult to be leaked through the 3D conduction if the volume of airgap is larger. The variation of R therefore can be considered as an indicator of the variation of the damage thickness if the diameter is the same. To further analyse the relationship between R and h, Fig. 7 plots the scatters between them, which suggests that the relationship is not linear but approximately exponential. An exponential fitting was applied on the measurements and the relationship can be described by

$$R = -0.29e^{-\frac{h}{0.93}} + 0.6. \quad (7)$$

The fitting error is quantified by calculating the Pearson correlation coefficient (PCC), denoted by ρ, between the measured R and reconstructed R based on (7) using the known h. If PCC equals to 1, it indicates a perfect fitting. The fitting curve is represented by the red plot of Fig. 7, and the calculated PCC value is 0.999. Both observations suggest that the identified model (7) can well represent their relationship. To estimate the value of h using the measured R, the model (7) can be rewritten as

$$h = -0.93\ln\frac{R-0.6}{-0.29}. \quad (8)$$

It should be noted that the empirical model (8) is established only for this specified defect depth, size and material, any change of which requires to re-calculate the coefficients. However, it is expected that the model structure is similar.

B. *Results of the Sample 2*

This sample aims to evaluate the dependence between d and R when h is fixed. Fig. 8 shows a snapshot of the raw thermal image at time 10 s after the flash. The defects are marked as "(1)", "(2)", "(3)", "(4)", and "(5)" to represent the defect depth d of 1.0 mm, 1.5 mm, 2.0 mm, 2.5 mm, and 3.0 mm respectively, and the sampled sound area is marked as 'S'. The sampling procedure was identical as that for the Sample 1. The temperature decay for each defect and selected sound region, plotted in the logarithmic domain, are shown in Fig. 9. It is expected that the time of the temperature deviation occurs for each defect (t*) is different and increases following the increase of defect depth, which is caused by the difference of defect depth.

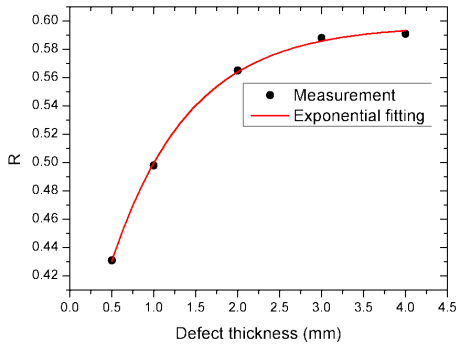

Fig. 7. The scatter plot between the defect thickness and the measured R with the corresponding exponential fitting for the Sample 1.

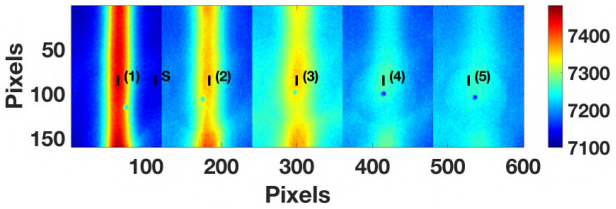

Fig. 8. A snapshot of the captured thermal image of at time 10 s for the Sample 2. The markers illustrate the 10 sampled pixels of each defect and sound area.

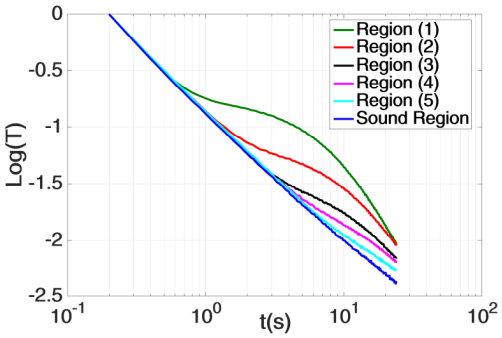

Fig. 9. The average temperature decay, plotted in the logarithmic domain, for the sampled pixels of each defect and a sound region of the Sample 2. The sampled total data length is 24 s.

The measured values of R and d by applying the NLSF method are shown in Table II. The absolute error of measured depth is 0.040±0.050 mm and the average percentage error is 2.2%. It has been observed that the value of R decreases following the increase of defect depth. Fig. 10 plots the scatters between R and d, which suggests the relationship is approximately linear. A linear fitting process was applied on the measurements and the relationship can be written by

$$R = -0.27d + 1.07. \quad (9)$$

The red plot of Fig. 10 illustrates the fitting and the PCC value is 0.993, both of which suggests the identified model (9) can well represent the relationship. It should be noted that the empirical model (9) is established only for the specified defect thickness, size and material, any change of which requires to re-calculate the coefficients. However, the linear model structure is expected.

TABLE II
ESTIMATED PARAMETERS OF THE SAMPLE 2

Defect depth (mm)	R	d (mm)
1.0	0.783	0.999
1.5	0.685	1.572
2.0	0.562	2.113
2.5	0.410	2.496
3.0	0.249	2.991

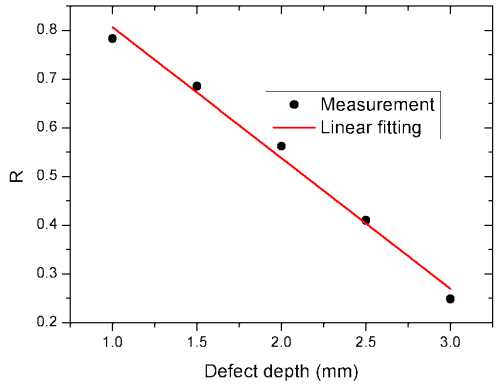

Fig. 10. The scatter plot between the defect thickness and the measured R with the corresponding linear fitting for the Sample 2.

The above results show that the value of R depends on both the defect depth and thickness. The dependence on depth is linear, and the dependence on thickness is nonlinear. The models (7) and (9) have a single input and single output, which has limited applications due to the rigorous assumption.

To analysis how d and h together affect the value of R, the NFIR model (4) with two inputs was employed and the data in Table I and II were sampled. The identified model is written as

$$R = -0.37d + 0.07dh - 0.02h^2 + 1.11 \quad (10)$$

with a PCC value of 0.98. This result suggests that the R value can be well explained by the defect thickness and depth. To construct a model for predicting h based on the values of R and d measured by the NLSF method, h is considered as the system output of the NFIR model and R as the system input. The results produced from both samples, presented in Table I and II, were sampled, and the predictive model is identified as

$$h = 170.72 - 33.96R - 81.3d + 163.81R^2 + 9.44d^2 + 82.56Rd \quad (11)$$

with a PCC value of 0.75. To validate its performance of prediction, Table III shows the predicted values of h based on Eq. (11) using the estimated R and d, against the ground truth for the 10 defects in the Sample 1 and the Sample 2. Although the prediction is not perfect, the result clearly demonstrates the potential to predict the defect thickness using the introduced approach. There are a few potential reasons of the relatively large error: 1) the material properties of the Sample 1 and the Sample 2 are not identical due to the manufacturing deviation, which is usually greater for inhomogeneous materials (e.g. composites); 2) the second order polynomial model structure cannot fully represent the mechanism; 3) there are some other parameters apart from R and d to be included in model (11) to better estimate h. It is expected that the prediction performance will be further improved by including the size of defect in this model.

TABLE III
THE DEFECT THICKNESS COMPARISON OF 10 STUDIED DEFECT IN THE SAMPLE 1 AND THE SAMPLE 2 BETWEEN THE GROUND TRUTH AND PREDICTION USING THE MODEL (11).

Defect ID	Ground Truth (mm)	Prediction (mm)	Error (mm)
Sample 1-1	0.5	1.34	0.84
Sample 1-2	1.0	1.23	0.23
Sample 1-3	2.0	1.56	0.44
Sample 1-4	3.0	3.68	0.68
Sample 1-5	4.0	2.54	1.46
Sample 2-1	1.5	1.47	0.03
Sample 2-2	1.5	1.95	0.45
Sample 2-3	1.5	1.25	0.25
Sample 2-4	1.5	1.53	0.03
Sample 2-5	1.5	1.45	0.05

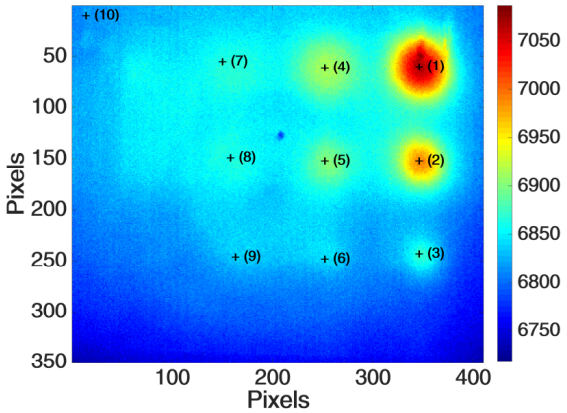

Fig. 11. A snapshot of the captured thermal image of at time 10 s for the Sample 3.

C. *Results of the Sample 3*

This sample aims to investigate how the geometrical parameters of flat-bottom holes affect the thermal reflection coefficient. It should be noted that the definition of "defect thickness" for this case is slightly different with the previous two cases since the defects are open on the back-side. We can consider this parameter as a representation of defect volume when the diameter is fixed, which is applicable to the Sample 1 and the Sample 2. A snapshot of the raw thermal image at time 10 s is shown in Fig. 11, where nine holes on top right side can be easily spotted while the holes with 4 mm depth and 5 mm diameter cannot be clearly detected due to low diameter to depth (aspect) ratios. Beemer and Shepard [28] acknowledges the difficulty in detecting flat-bottom holes if the aspect ratios is smaller than 5. For this reason, in this experiment, only the nine marked holes in Fig. 11 were studies. Fig. 12(a) plots the temperature decay of the sampled pixels "1", "2", and "3" which have the same defect depth of 1 mm but with different defect size (20 mm, 15 mm, and 10 mm respectively). The point "10" was randomly sampled from the sound region. As expected, the values of t* for the considered three defects are similar, and the cooling behaviours between t* and t** are different due to the difference of size. Fig. 12(b) plots the temperature decay of the sampled defects "1", "4",

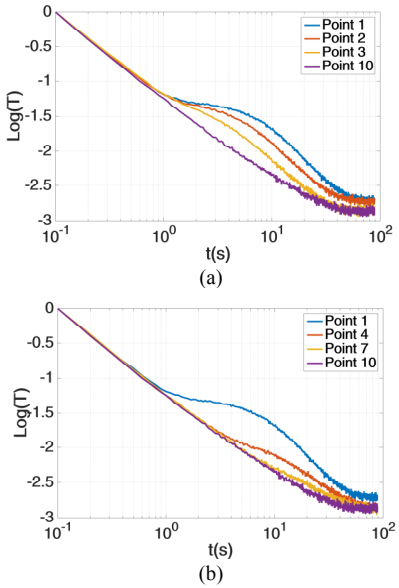

Fig. 12. The temperature decay, plotted in the logarithmic domain, for the selected defects and sound pixel. (a) the defects have the same depth but different size, (b) the defects have the same size but different depth.

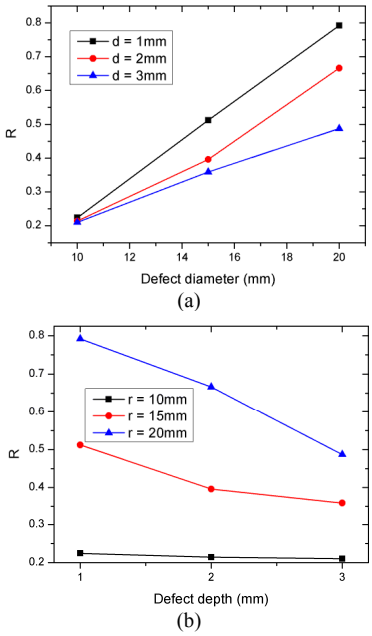

Fig. 13. Results of the Sample 3. (a) The scatter plot between the defect diameter and the measured R, (b) the scatter plot between the defect depth and the measured R.

and "7" which have the same defect size of 20 mm but with different defect depth (1 mm, 2 mm, and 3 mm respectively). Both the value of t* and the cooling behaviours of [t*, t**] are different due to the difference of size and depth.

The measured values of R and d by applying the NLSF method are shown in Table IV. It can be observed that the depth can be estimated satisfactorily with an absolute error of 0.033±0.025 mm, and the average percentage error is 2.3%. It has also been observed that the larger diameter of defects leads to higher value of R, and the deeper defect leads to the smaller value of R. This observation is similar as that of the Sample 2. To further understand their relationship, Fig. 13(a)

TABLE IV
ESTIMATED PARAMETERS OF THE SAMPLE 3

Defect depth (mm)	r: 10 mm		r: 15 mm		r: 20 mm	
	R	d (mm)	R	d (mm)	R	d (mm)
1.0	0.224	0.926	0.512	1.011	0.792	1.072
2.0	0.214	1.974	0.396	1.991	0.666	2.029
3.0	0.210	2.968	0.359	3.005	0.487	2.962

TABLE V
THE DEFECT THICKNESS COMPARISON OF 9 STUDIED DEFECT IN THE SAMPLE 3 BETWEEN THE GROUND TRUTH AND PREDICTION USING THE MODEL (13).

Defect ID	Ground Truth (mm)	Prediction (mm)	Error (mm)
Sample 3-1	7	6.17	0.83
Sample 3-2	6	5.96	0.04
Sample 3-3	5	5.87	0.87
Sample 3-4	7	7.24	0.24
Sample 3-5	6	5.63	0.37
Sample 3-6	5	5.13	0.13
Sample 3-7	7	6.91	0.09
Sample 3-8	6	6.09	0.09
Sample 3-9	5	5.00	0.00

plots the R value against the defect diameter for three defect depths, where the relationship was observed as approximately linear. Fig. 13(b) plots the R value against the defect depth for three defect diameters, where the relationship was also observed as approximately linear. This observation is very similar with that shown in Fig. 10 for the Sample 2. The sensitivity of the R value on the defect depth increases following the increase of defect size. The R values are almost same for the defects with the diameter of 10 mm. To fully reveal their relationship, an NFIR model was identified and is written as

$$R = 0.043r - 0.079d - 0.062, \quad (12)$$

which confirms the relations between R and r, and R and d are approximately linear. The calculated PCC value is 0.965, which suggests an excellent performance of the model. The prediction of h, equivalent to the prediction of d, can be written as

$$h = 3.14 - 37.18R + 1.77r - 1.67R^2 - 0.06r^2 + 1.65Rr \quad (13)$$

with a PCC value of 0.85. To evaluate the performance of the model (13), Table V shows the predicted values and the ground truth of h for the 9 defects in the Sample 3. The result clearly demonstrates that the measured R value has a potential to predict the defect thickness for flat-bottom holes through considering the defect diameter.

V. CONCLUSIONS

Different with most of degradation assessment research focusing on damage/defects detection and depth measurement, this paper addresses the challenge to measure the damage thickness based on a single-side inspection of pulsed thermography under the reflection mode. This paper proposes to use the thermal reflection coefficient (R) and measurable geometrical parameters of the damage, including size and depth, to predict the thickness using a Nonlinear Finite Impulse Response (NFIR) model. Applications of the proposed approach on three CFRP laminates show that:

a. The proposed method considerably improves the

degradation assessment performance by extending the measurement of damage/defects from two dimensions to three dimensions.

b. For a specific material, the R value is strongly correlated with the defect size, depth and thickness. It has been observed that the relationship of R with the defect depth and the relationship of R with the defect size are approximately linear, while that for R and the defect thickness is approximately exponential. This observation allows deriving an empirical model to establish their independence, which enables the quantification of defect thickness using a single-side pulsed thermographic inspection.
c. The identified NFIR models demonstrated the potential to predict the defect thickness using R and other measurable physical parameters. The Pearson Correlation Coefficients of the prediction for block defects and flat-bottom holes are 0.75 and 0.85, respectively.

With this developed approach, the interlaminar bond integrity of composite joints can be better evaluated through accurately measuring the thin airgaps in the interface of dissimilar polymer composite materials. The single-side inspection not only reduces the inspection time, but also extends the application on components where one side is not accessible. A potential disadvantage of this approach is that the air gap thickness is a function of multiple correlated parameters, which may limit its application on irregular airgaps. One potential solution is to use the Principle Component Analysis to select the most important parameter to simplify the model or convert to a function of multiple independent parameters.

It should be noted that this paper is a feasibility study and the performance of the identified models is limited on the produced specimens. The change of materials or defect shape may have influence on the results. To fully explore its potential and improve the versatility of the identified model, a further study is required by considering different materials with a variety of defect shape, size, thickness and depth. Furthermore, this paper neglects the influence of adjacent defect on results, although which has been mitigated during the sample design by leaving a relatively large space between defects. Full industrialisation of the proposed technique requires examination of it in actual applications.

REFERENCES

[1] H. Yazdani Nezhad, Y. Zhao, P. D. Liddel, V. Marchante, and R. Roy, "A novel process-linked assembly failure model for adhesively bonded composite structures," *CIRP Ann. - Manuf. Technol.*, vol. 66, no. 1, pp. 29–32, 2017.

[2] A. Baker, A. J. Gunnion, and J. Wang, "On the Certification of Bonded Repairs to Primary Composite Aircraft Components," *J. Adhes.*, vol. 91, no. 1–2, pp. 4–38, Jan. 2015.

[3] R. Bhanushali, D. Ayre, and H. Y. Nezhad, "Tensile Response of Adhesively Bonded Composite-to-composite Single-lap Joints in the Presence of Bond Deficiency," *Procedia CIRP*, vol. 59, no. TESConf 2016, pp. 139–143, 2017.

[4] H. Y. Nezhad, F. Merwick, R. M. Frizzell, and C. T. McCarthy, "Numerical analysis of low-velocity rigid-body impact response of composite panels," *Int. J. Crashworthiness*, vol. 20, no. 1, pp. 27–43, Jan. 2015.

[5] E. V. González, P. Maimí, P. P. Camanho, A. Turon, and J. A. Mayugo, "Simulation of drop-weight impact and compression after impact tests on composite laminates," *Compos. Struct.*, vol. 94, no. 11, pp. 3364–3378, Nov. 2012.

[6] D. Pieper, K. M. Donnell, M. T. Ghasr, and E. C. Kinzel, "Integration of microwave and thermographic NDT methods for corrosion detection," 2014, pp. 1560–1567.

[7] H. Zhang, R. Yang, Y. He, A. Foudazi, L. Cheng, and G. Tian, "A Review of Microwave Thermography Nondestructive Testing and Evaluation," *Sensors*, vol. 17, no. 5, p. 1123, May 2017.

[8] P. Wang, Z. Li, L. Zhou, and Y. Pei, "Microwave nondestructive detection and quantitative evaluation of kissing defects in GFRP laminates," *Compos. Sci. Technol.*, vol. 162, pp. 117–122, Jul. 2018.

[9] G. Singh, H. M. Bapat, B. P. Singh, M. Bandyopadhyay, R. K. Puri, and D. N. Badodkar, "Thickness Evaluation of Aluminium Plate Using Pulsed Eddy Current Technique," *J. Inst. Eng. Ser. D*, vol. 94, no. 2, pp. 89–93, Oct. 2013.

[10] S. Dixon, P. A. Petcher, Y. Fan, D. Maisey, and P. Nickolds, "Ultrasonic metal sheet thickness measurement without prior wave speed calibration," *J. Phys. D. Appl. Phys.*, vol. 46, no. 44, p. 445502, Nov. 2013.

[11] S. C. Garcea, Y. Wang, and P. J. Withers, "X-ray computed tomography of polymer composites," *Compos. Sci. Technol.*, vol. 156, pp. 305–319, Mar. 2018.

[12] V. P. Vavilov and D. D. Burleigh, "Review of pulsed thermal NDT: Physical principles, theory and data processing," *NDT E Int.*, vol. 73, pp. 28–52, 2015.

[13] Y. Zhao, S. Addepalli, A. Sirikham, and R. Roy, "A confidence map based damage assessment approach using pulsed thermographic inspection," *NDT E Int.*, vol. 93, pp. 86–97, Jan. 2018.

[14] X. P. Maldague, *Theory and Practice of Infrared Technology for Nondestructive Testing*. New York: Wiley, 2001.

[15] X. Han, L. D. Favro, P. K. Kuo, and R. L. Thomas, "Early-Time Pulse-Echo Thermal Wave Imaging," in *Review of Progress in Quantitative Nondestructive Evaluation*, Boston, MA: Springer US, 1996, pp. 519–524.

[16] S. M. Shepard, J. R. Lhota, B. a. Rubadeux, D. Wang, and T. Ahmed, "Reconstruction and enhancement of active thermographic image sequences," *Opt. Eng.*, vol. 42, no. 5, pp. 1337–1342, 2003.

[17] Z. Zeng, J. Zhou, N. Tao, L. Feng, and C. Zhang, "Absolute peak slope time based thickness measurement using pulsed thermography," *Infrared Phys. Technol.*, vol. 55, no. 2–3, pp. 200–204, 2012.

[18] Y. Zhao, J. Mehnen, A. Sirikham, and R. Roy, "A novel defect depth measurement method based on Nonlinear System Identification for pulsed thermographic inspection," *Mech. Syst. Signal Process.*, vol. 85, pp. 382–395, Feb. 2017.

[19] J. G. Sun, "Analysis of Pulsed Thermography Methods for Defect Depth Prediction," *J. Heat Transfer*, vol. 128, no. 4, p. 329, 2006.

[20] A. Sirikham, Y. Zhao, and J. Mehnen, "Determination of thermal wave reflection coefficient to better estimate defect depth using pulsed thermography," *Infrared Phys. Technol.*, vol. 86, pp. 1–10, 2017.

[21] S. M. Shepard, M. Frendberg, and Y. L. Hou, "Characterization of Full-Range Time Evolution in Active Thermography," in *12th International Conference on Quantitative Infrared Thermography (QIRT)*, 2012.

[22] S. K. Lau, D. P. Almond, and J. M. Milne, "A quantitative analysis of pulsed video thermography," *NDT E Int.*, vol. 24, no. 4, pp. 195–202, 1991.

[23] A. Sirikham, Y. Zhao, and J. Mehnen, "Determination of thermal wave reflection coefficient to better estimate defect depth using pulsed thermography," *Infrared Phys. Technol.*, vol. 86, pp. 1–10, Nov. 2017.

[24] S. A. Billings, *Nonlinear System Identification*. Chichester, UK: John Wiley & Sons, Ltd, 2013.

[25] S. Chen and S. A. Billings, "Representations of non-linear systems: the NARMAX model," *Int. J. Control*, vol. 49, no. 3, pp. 1013–1032, Mar. 1989.

[26] Y. Zhao, S. A. Billings, H. Wei, and P. G. Sarrigiannis, "Tracking time-varying causality and directionality of information flow using an error reduction ratio test with applications to electroencephalography data," *Phys. Rev. E*, vol. 86, no. 5, p. 051919, Nov. 2012.

[27] S. Dudzik, "A simple method for defect area detection using active thermography," *Opto-Electronics Rev.*, vol. 17, no. 4, Jan. 2009.

[28] M. F. Beemer and S. M. Shepard, "Aspect ratio considerations for flat bottom hole defects in active thermography," *Quant. Infrared Thermogr. J.*, vol. 6733, no. June, pp. 1–16, 2017.

2018-10-31

Estimation of damage thickness in fibre-reinforced composites using pulsed thermogra

Sirikham, Adisorn

Sirikham A, Zhao Y, Yazdani Nezhad H, et al., (2019) Estimation of damage thickness in fibre-reinforced composites using pulsed thermography. IEEE Transactions on Industrial Informatics, Volume 15, Issue 1, January 2019, pp. 445-453

https://doi.org/10.1109/TII.2018.2878758